Control of the critical current density in $YBa_2Cu_3O_{7-\delta}$ films by means of intergrain and intragrain correlated defects

E. Mezzetti, R. Gerbaldo, G. Ghigo, L. Gozzelino, and B. Minetti
INFM–Torino-Politecnico, INFN–Torino and Politecnico di Torino, c.so Duca degli Abruzzi 24, 10129 Torino, Italy

C. Camerlingo and A. Monaco
Istituto di Cibernetica del Consiglio Nazionale delle Ricerche, Via Toiano 6, 80072 Arco Felice, Italy

G. Cuttone and A. Rovelli
Laboratori Nazionali del Sud–INFN, via S. Sofia 44, 95123 Catania, Italy
(Received 13 January 1999)

The aim of this work is to investigate the mechanisms controlling the current-carrying capability of $YBa_2Cu_3O_{7-\delta}$ thin films. A comparison between the magnetic properties of a film with intrinsic grain-boundary defects and two films crossed by columnar defects with different densities is presented. Such properties have been studied by means of ac susceptibility measurements, resistivity measurements, and structural characterizations. The Clem and Sanchez model [Phys. Rev. B **50**, 9355 (1994)] is used to extract critical current values from the susceptibility data. In the virgin film, correlated grain-boundary defects were created among islands with homogeneous size, by means of the appropriate modifications in the growth process. Columnar defects were produced through 0.25-GeV Au-ion irradiation. The central issue concerns the investigation of the plateaulike features characterizing the log-log field dependence of the critical current density, the analysis of the J_c temperature dependence, and of the irreversibility line. An analytical expression of J_c vs B is given in order to compare the main issues with the experimental data. This model suggests that the *intergrain* pinning dominates in the high-current/low-temperature regime through a network of frustrated Josephson junctions, while the *intragrain* pinning is effective near the irreversibility line.
[S0163-1829(99)12433-0]

I. INTRODUCTION

The critical current density in high-T_c superconducting (HTS) films is typically higher than in single crystals,[1] due to the presence of a larger number and variety of defects that may act as pinning centers. A stronger flux pinning results in a smoother dependence of the critical current density (J_c) on the magnetic field, which is a crucial property to investigate, both for fundamental understanding and for practical applications.

Enhanced critical currents as well as plateaulike features in $J_c(B)$ log-log plots can be obtained by optimizing the growth process in order to produce suitable defects.[2,3] An alternative strategy is the implantation of extrinsic defects, e.g., by means of irradiation.[4–6] Particularly the case of linearly correlated defects (columnar defects) has been widely investigated, both experimentally and theoretically.[7–9]

The microstructure of sputtered $YBa_2Cu_3O_{7-\delta}$ (YBCO) films typically presents islands separated by trenches where the superconducting order parameter is reduced.[2,10] These boundary regions can provide strong flux pinning.[11–13] In the same way, twin boundaries at low temperatures provide strong pinning in single crystals.[14] A fundamental insight on these topics is given by the study of bicrystals in which vortex matching effects at the periodic facet structure across the boundary were observed.[12]

The aim of this work is to correlate the current-carrying capability of YBCO sputtered films with their defect distribution. In particular we analyze the plateaulike features in the log-log curve $J_c(B)$, i.e., the existence of a region in which $\log(J_c)$ is nearly independent on the logarithm of the field, followed by a J_c drop. In order to study these plateau features, we modified the pinning properties of the samples following two approaches: (i) by creating native defects in the material by appropriate modifications in the growth process; (ii) by introducing controlled defects by means of 0.25-GeV Au-ion irradiation, which induces columnar tracks crossing the whole sample. The modification of the growth process leads to the production of slightly underdoped films. As revealed by the ''tail regime'' in the $R(T)$ transition and by structural analysis, a slight deoxygenation results in the formation of defected grain boundaries (GB's). Many as-grown correlated defects nucleate at the intersection of the trenches separating islands, as discussed below. We compare the critical current behavior as a function of field and temperature in the as-grown film with the corresponding trends in films irradiated at two different doses. The chosen irradiation dose in the first case corresponds to a defect density close to the density of the islands. The second dose was selected five times higher. The discussion of the data is centered on the characteristic features of the J_c vs B and vs T curves, looking at the correlations between these features and the defect distributions. The crucial task is to determine whether the really effective pinning centers lie along the GB's and/or inside the islands, and which one is responsible for the matching conditions between the vortex lattice and the correlated-defect structure. The regime of low currents, and in particular the possible shifts of the irreversibility line

due to ion-induced columnar defects, is also explored and discussed.

The measure of the susceptibility is used to investigate the magnetic behavior and to extract critical current density values. Information about the structural properties is obtained by x-ray diffractometry (crystalline orientation), Raman analysis (oxygen content), and atomic force microscopy (AFM) analysis (surface morphology).

II. EXPERIMENTAL

The $YBa_2Cu_3O_{7-\delta}$ superconducting films were fabricated *in situ* by dc sputtering from inverted cylindrical magnetron on $SrTiO_3$ (100) oriented substrates. Since we aimed at studying YBCO films with defected GB's, we slightly modified the standard growth process. The grain size and the boundary properties can be controlled, preserving the crystalline orientation, by varying the cooling rate. This procedure leads to an underdoped state, which we presume to be responsible for the slightly lower critical temperature observed.[15]

During deposition an Ar/O_2 (4:3) gas mixture with a total pressure of 93 Pa was used, with a dc power of 110 W, resulting in a growth rate of about 2 nm/min. The substrates were glued to a vacuum heater by silver paint and heated during deposition at a temperature $T_S = 820\,^{\circ}\mathrm{C}$. In order to improve the temperature uniformity and stability, a 900-nm-thick Au film was deposited on the substrate back side. Two films were produced: one using the standard cooling process (F), one using a slightly modified cooling process in order to obtain YBCO films with unambiguously defected GB's (D). For the (F) film, after deposition the vacuum chamber was filled with oxygen at a pressure of 40 kPa and the heater power was slowly decreased, cooling the sample at a rate of 10 °C/min until $T_S = 600\,^{\circ}\mathrm{C}$ was reached. After a rest of 15 minutes, the O_2 pressure was raised to 80 kPa and the sample temperature was decreased at a slower rate (5 °C/min) to 450 °C and kept at this temperature for 60 minutes; then the heater was turned off. This standard cooling procedure allows for the fabrication of full oxygenated YBCO films with high critical temperature ($T_c = 91.0$ K). For the (D) film, after deposition the vacuum chamber was filled with 80 kPa of oxygen and the temperature was slowly decreased (10 °C/min) until the temperature $T_S = 450\,^{\circ}\mathrm{C}$ was reached. After a rest of 30 minutes the heater was turned off. Two sets of samples were obtained, each from a single deposition, by cutting the film (F) and (D), respectively. This paper is focused on the analysis of (D) samples, while the (F) samples are used for the sake of comparison.

The crystal structure of the (D) film was analyzed by conventional θ-2θ x-ray diffractometer and reciprocal space mapping, using a multicrystal diffractometer (Philips MRD). The divergence of the incident beam was reduced to 12 seconds by a four-crystal Ge (220) monochromator. A conventional Cu target was used as x-ray source (3-kW generator). The Raman spectra were revealed by the Raman microprobe apparatus Dilor LabRam of ISA, using HeNe laser light excitation. The surface morphology was investigated by atomic force microscopy by using a Si_3N_4 tip. The electrical resistance was measured by the four contact method. Magnetic susceptibility measurements were carried out by means of a commercial ac susceptometer. Both ac and dc fields were oriented parallel to the sample *c* axis and to the irradiation tracks.

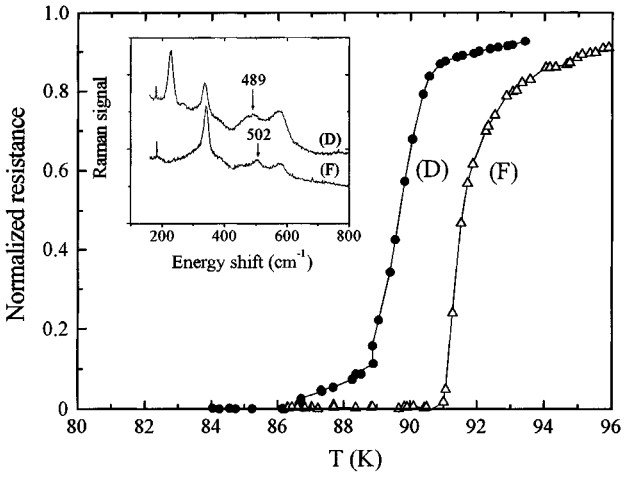

FIG. 1. Resistive transition for fully oxygenated (F) and underdoped (D) YBCO films. The inset shows the corresponding Raman spectra. Arrows mark the positions of the peaks used for the determination of the oxygen content.

0.25-GeV ^{197}Au-ion irradiations were performed at room temperature and in vacuum at the 15-MV Tandem accelerator of the INFN-Laboratori Nazionali del Sud (Catania, Italy). The samples were irradiated perpendicularly to the surface with fluences $\Phi = 1.5\times10^{10}$ and 7.5×10^{10} ions/cm^2, corresponding to dose equivalent fields[16] $B_\phi = 0.3$ and 1.5 T, respectively. TRIM code[17] simulations show that the energy released during the scattering processes in the whole thickness of the film overcomes the threshold of 20 MeV/μm, which is considered to be the lowest limit for the production of continuous tracks in YBCO.[18] The effective defect diameter usually obtained by heavy-ion irradiation on YBCO ranges from 5–10 nm.[19,20]

III. STRUCTURAL AND RESISTIVE CHARACTERIZATIONS

The resistance dependence on the temperature of the YBCO films is shown in Fig 1. The resistance is normalized to the value measured at $T = 100$ K. The curve (D) refers to the samples prepared with the modified cooling process, as those used in the irradiation experiments in this paper. It exhibits a pronounced resistance tail for temperatures below the main resistance drop, which is absent in the $R(T)$ curve of the fully oxygenated film (F), reported in the figure for the sake of comparison.

The oxygen content was inferred from Raman measurements, by the position of the line ν_H (marked by arrows in the inset of Fig. 1) due to the apical oxygen vibration mode. Using the relationship given by Huong,[21] $\delta = 0.025\nu_H - 5.57$ for δ in $YBa_2Cu_3O_{7-\delta}$ formula, the values $\delta = 0.34$ and $\delta = 0.02$ were estimated for films (D) and (F), respectively. The large Raman line appearing in the spectra of samples (D) at 230 cm^{-1} and the broad band at 580 cm^{-1} can be attributed to vibration modes associated with oxygen defects.[22,23] Although the exact origin of these Raman modes is not clear yet,[24] for slightly oxygen deficient YBCO (δ

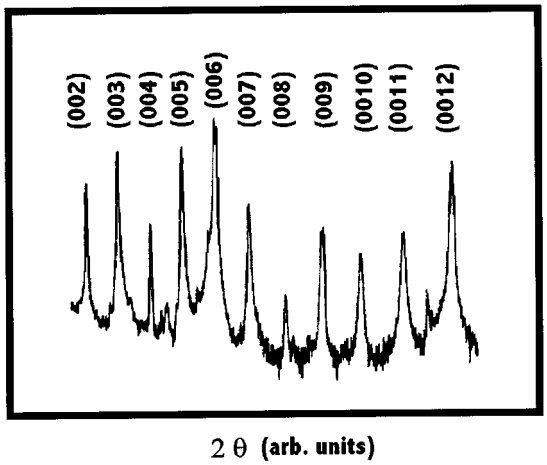

FIG. 2. θ-2θ x-ray diffractogram for the slightly oxygen-deficient YBCO films produced with the process (D).

$=0.3-0.4$) these modes are associated mainly with oxygen vacancies in the CuO chains.[25] The samples (D) exhibit disorder in the oxygen sublattice, with broken CuO chains and probably the setup of out-of-phase oxygen microdomains.[23]

These features do not affect the crystalline properties of the films, which exhibit a strong crystal orientation in the θ-2θ x-ray diffractogram, with c axis directed normal to the surface plane, as reported in Fig. 2. The crystalline perfection is confirmed by the ϕ-map x-ray analysis, which shows a strong correlation between the film and the underlying $SrTiO_3$ substrate lattice, with a small spread of the in-plane direction of a and b axis of the film grains. Hence we assume that our YBCO films nucleate on the $SrTiO_3$ substrate in the form of c-axis oriented single-crystalline islands. The island structure is clearly visible in the initial growth stage of the film. Figure 3 reports the AFM image of a 50-nm-thick (D) sample. The surface morphology consists in islands about 100 nm in diameter.

As previously mentioned, the oxygen miscomposition is also responsible for the tail regime, clearly visible in the $R(T)$ curve of the samples (D). The slow approach to the zero resistance state is the signature of a suppression of the order parameter in the GB region.[11] On the other hand, the susceptibility characterization of these films (presented below) does not show the double transition typical of weakly coupled granular materials. Hence we assume that the samples under investigation present GB's which do not behave as weak links.[26,10]

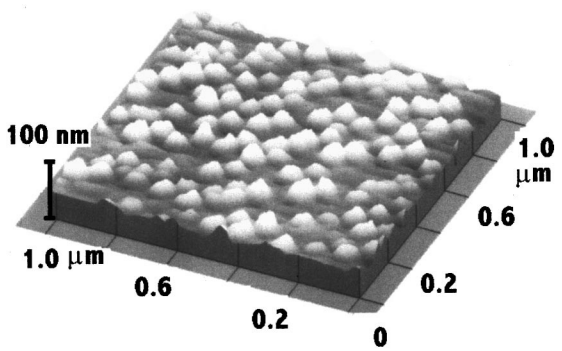

FIG. 3. AFM image showing the surface morphology of a 50-nm-thick film.

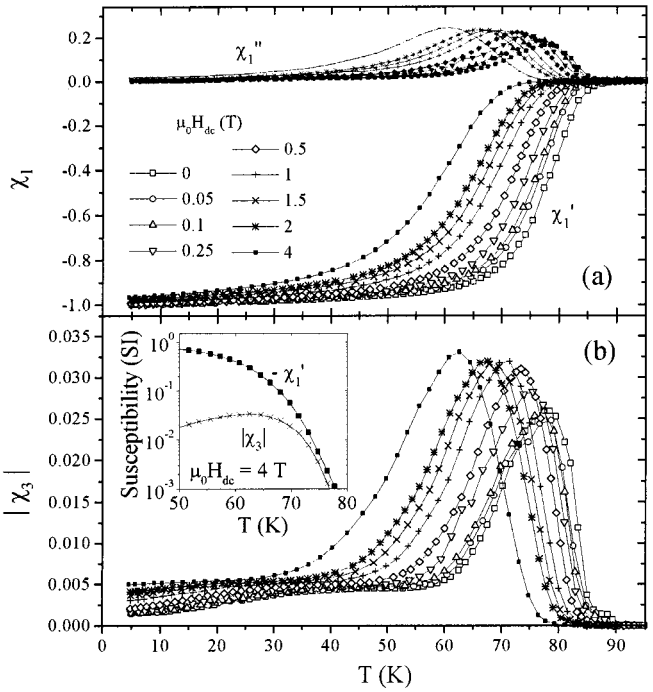

FIG. 4. Typical results of first (a) and third (b) harmonic ac susceptibility measured for different dc fields, listed in the figure.

The GB network itself constitutes a network of planar defects.[26] Moreover, simple topological considerations show that the meeting point of three or more islands constitutes a columnarlike defect site along the film thickness. Other linearly correlated defects could originate as linear dislocations in low-angle GB's,[27] or as dislocation chains.[28] Although all these defects are less controllable than ion-induced defects, they are effective in determining the pinning capability of these films.

IV. SUSCEPTIBILITY MEASUREMENTS

Figure 4 shows typical results of first and third harmonic ac susceptibility χ, measured in different dc fields. All experimental data were divided by the value χ_0 which normalizes to -1 the real part of the susceptibility measured for $H_{dc}=0$ at $T=4.2$ K, i.e., in conditions of complete shielding. The application of an external dc field results in a shift of the curve towards lower temperatures. Critical temperature values were evaluated as the values where the Re(χ) signal significantly emerges from the noise (1% of the signal at $T=4.2$ K). Ion-induced defects crossing the whole sample lead to a T_c decrease, from $T_c=88$ K (virgin film) to $T_c=83.8$ K (low-dose irradiated film) and to $T_c=82.3$ K (high-dose irradiated film). The T_c decrease can be ascribed to a further disorder in the oxygen sublattice and to the presence of amorphous tracks that affect a significant fraction of the material. In this case, the shift is higher than expected,[29] probably due to the preirradiation oxygen deficiency. In order to stress the flux-pinning properties due to defects, we present our results as a function of the reduced temperature T/T_c.

First harmonic susceptibility data were analyzed in the framework of the Clem and Sanchez model for the case of a thin sample in a transverse field.[30] We extracted the values of

the critical current density by numerically inverting the relation

$$\chi' = \frac{2\chi_0}{\pi}\int_0^{\pi}(1-\cos\vartheta)S[(x/2)(1-\cos\vartheta)]\cos\vartheta\, d\vartheta$$

with

$$S(x) = \frac{1}{2x}\left[\cos^{-1}\left[\frac{1}{\cosh x}\right] + \frac{\sinh x}{\cosh^2 x}\right],$$

where $x = 2h_0/(J_c t)$, h_0 is the amplitude of the ac field, and t is the sample thickness. The application of a dc field does not modify this expression as long as the critical current is weakly field dependent. The validity of this model was checked by comparing the experimental Im(χ) vs Re(χ) plots with the model predictions. The critical current density values reported in this work were extracted in field and temperature ranges which satisfy the model constraints.

The third harmonic component χ_3 in the susceptibility signal reflects the high nonlinearity of the current-voltage characteristics, i.e., the presence of current-dependent barriers for flux motion, as in the case of a pinned vortex lattice. The absence of a third harmonic signal implies a linear response, as in the case of flux lines in a liquid state. The irreversibility line, which is the line of vanishing depinning critical current, was therefore determined by the onset temperature of the χ_3 signal.

V. RESULTS AND DISCUSSION

A. Magnetic field dependence of the critical current density

We analyzed three samples, labeled (a), (b), and (c). The sample (a) is the reference film. The sample (b) was irradiated up to a dose equivalent field[16] $B_\phi = 0.3$ T, corresponding to an average distance between tracks $d = 83$ nm [$d = (\Phi_0/B_\phi)^{1/2}$ where Φ_0 is the flux quantum]. In this case, the chosen average distance between the tracks and the island diameter are of the same order of magnitude. The film (c) was irradiated at a quite larger dose ($B_\phi = 1.5$ T). The corresponding average distance between the tracks is $d = 37$ nm, significantly lower than the estimated distance between defects in the two other films.

As mentioned above, we focus on the analysis of the plateaulike features in the log-log curve $J_c(B)$. For this reason we perform specific χ measurements in a wide range of fields, at seven reduced temperatures. Figure 5 shows the field dependence of J_c at $T/T_c = 0.32$ for the as-grown sample. Two different regimes can be distinguished. For low fields the critical current density varies slowly, while a clear J_c drop appears at about $\mu_0 H = 0.3$ T. The existence of such a characteristic plateaulike feature, followed by a steeper drop, is usually related to particularly favorable pinning conditions, although in the case of HTS films these mechanisms are not fully understood yet.[1,31–33]

First we look at these behaviors in the general framework of correlated disorder models.[7–9] In the case of columnar defects, characteristic features usually emerge due to the existence of matching conditions between the vortex lattice and the defect structure. It was found that, when the fluxon density is lower than the defect density, dissipation only occurs

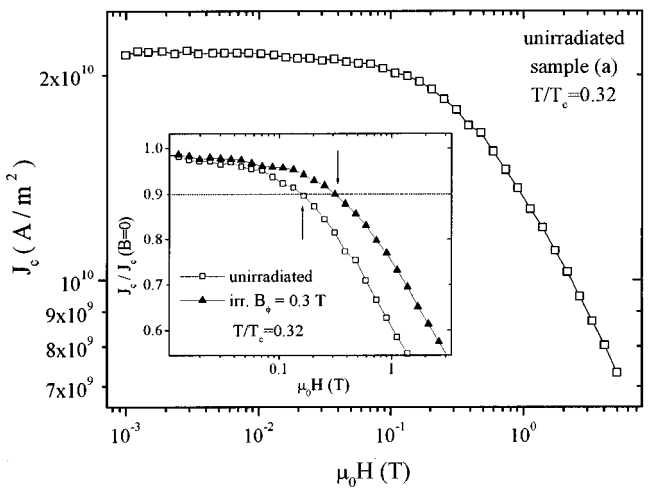

FIG. 5. Critical current density as a function of the magnetic field for $T/T_c = 0.32$. In the inset the critical current densities, normalized to the value measured in zero dc field, are reported for the reference sample (a) and for the sample (b), irradiated at $B_\phi = 0.3$ T. Arrows mark the values of B^* (see text) for the two curves.

due to variable-range-hopping excitations. If columnar pins are periodically distributed, this regime is extended up to the defect equivalent field B_ϕ, corresponding to a complete matching between vortex and column lattices. When B_ϕ is exceeded, interdefect potential wells, due to vortex-vortex repulsion, are usually too weak to prevent vortex motion or flux-lattice instability. If pins are dense and some randomness is introduced, vortex-vortex interactions play a dominant role, and the matching conditions are more complex.[34] For the case of ion irradiated YBCO single crystals, the problem was studied by L. Krusin-Elbaum *et al.*,[35] who defined an ''accommodation field'' as the field $B^* < B_\phi$ above which $J_c(B) \sim B^{-1}$. They experimentally observed that this definition corresponds to a $J_c(B)/J_c(0) \approx 0.63$ criterion.

In our case, aiming at studying the onset of the $J_c(B)$ drop in the presence of large plateaulike features, it is more convenient to choose a higher threshold to separate the two mentioned regimes, i.e., to define B^* as the field at which the critical current reaches the 90% of the value obtained for zero applied field. In the inset of Fig. 5, $J_c(B)/J_c(0)$ curves for the irradiated sample (b) and the unirradiated sample (a) are reported. The effect of ion irradiation in the high current regime is just an enhancement of the B^* field, indicated by the arrows. In Fig. 6 the dependence of B^* on the reduced temperature for the three samples is shown. The right-hand scale reports the average distance between vortices corresponding to the fields B^*. The curve of the reference sample (a) shows a weak dependence on temperature in the range $T/T_c = 0.32-0.53$. The B^* fields in this range correspond to an intervortex average distance $d = 120$ nm. This value is of the same order of magnitude of the island diameter shown in Fig. 3. In the temperature range where B^* is nearly independent of the temperature, the accommodation of the vortices inside the defect lattice reaches its optimal conditions.

The curves $B^*(T)$ of samples (b) and (c) exhibit higher B^* values at low temperatures and do not present plateaulike features in the considered temperature range. This qualitatively different behavior is expected and can be explained by

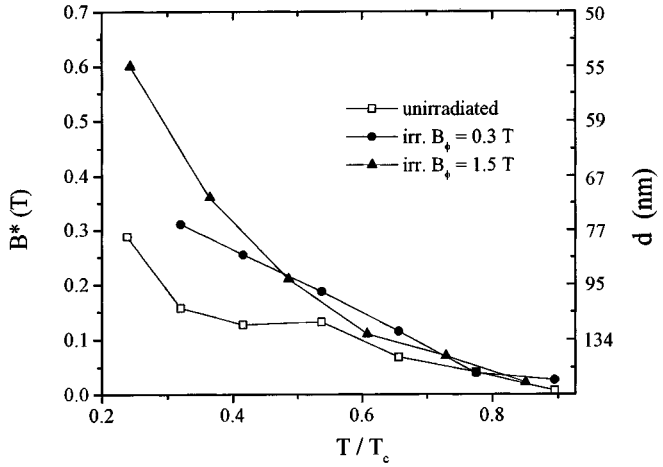

FIG. 6. Value of B^* (see text) as a function of the reduced temperature, for the reference sample (a) and for samples (b) and (c), irradiated at $B_\phi = 0.3$ and 1.5 T, respectively. The right-hand scale reports the average intervortex distance corresponding to the B^* values.

the fact that columnar defects allow to shift the optimal conditions towards the dose equivalent field B_ϕ.[36]

B. Temperature dependence of the critical current density

The analysis of the temperature dependence of the critical current density provides further insights on the nature and role of the accommodation fields in the case of films. In particular, sample (c) allows to analyze the temperature decay of the critical current density in the context of a density of linearly correlated defects quite higher than the virgin film (Fig. 7). In the high-temperature regime, the $J_c(T/T_c)$ curves measured on film (a) and film (c) at the same field roughly overlap (inset). As the temperature is decreased towards the lower limit, the performances of the irradiated sample improve, and a remarkable characteristic appears (main figure). The data obtained for sample (c) in a field of 0.5 T overlap with the values obtained for sample (a) in zero field. Exactly the same trend is shown by the curves measured at $B = 1$ and 4 T, which overlap on the reference curves measured at $B = 0.05$ and 2 T, respectively. This means that additional vortices, up to a number proportional to the field difference between overlapping curves, do not produce additional dissipation. Other combinations of fields that produce overlapping curves could in principle be found, but we have investigated only a limited number of fields.

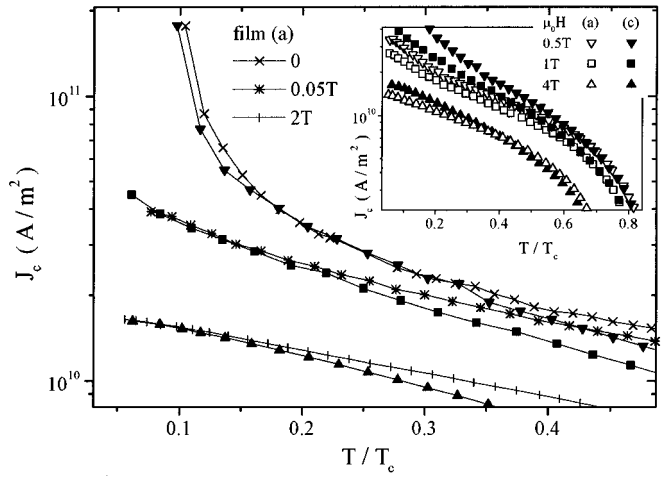

FIG. 7. Critical current density vs reduced temperature for the reference sample (a) and for the irradiated sample (c) ($B_\phi = 1.5$ T), at different applied fields. The curves obtained for the two films in the same fields overlap only in the high-temperature region (inset). The main figure reports the $J_c(T/T_c)$ curves for the film (c) (the same data of the inset) in the low-temperature region. In this case the comparison is made with the curves obtained for the film (a) at those fields that produce the same J_c values at the lowest temperatures.

A possible framework to explain these results is based on the existence of a hidden intergranular network among strongly coupled islands. This network could be interpreted as an intergranular network of long Josephson junctions (LJJ), with coupling energies modulated by the presence of defects, both intrinsic and extrinsic.[32,33] In this case a LJJ with columnar defects is equivalent to a row of short Josephson junctions.[37] Itzler and Tinkham found that in the vicinity of a commensurate-field value, the current-voltage curves of a junction with periodic defects recover all the characteristics they had near zero field.[38] In a similar framework, Fehrenbacher, Geshkenbein, and Blatter showed that in the case of random-distributed defects these matching conditions are valid in a certain range of fields, so that a continuous spectrum of fields can be accommodated up to a maximum, once the defect distribution and size are fixed.[32] As emphasized above, the peculiar characteristic of the defects to provide recovering of the zero-field performances in high fields is exhibited by our results at low temperatures for sample (c). It is worthwhile to mention that the recovery of zero-field performances in matching fields was also observed in bulk polycrystalline YBCO samples irradiated with 6.5-MeV protons.[39] In that case, a suitable correlation of defects contributed to the pinning of vortices in the intergrain network. As it is shown in the next section, a hidden network of Josephson junctions is fully coherent with our present results, if defects of nanometric size and relative energy scales in the GB's are now considered.[33]

C. HTS films modeled as arrays of Josephson junctions

The results of the previous sections suggest that most of the boundary interfaces in our films are not usual weak links, normally responsible for the so-called magnetic granularity.[26] On the contrary, our GB's are high-J_c junctions, playing the role of ''hidden'' weak links. This assumption accounts for a strong proximity coupling across the defects.[26] Most of them are considered as insulating zones of nanometric size with modified carrier density and reduced order parameter. Transport of Cooper pairs through such layers occurs via tunneling. Inside the boundary interfaces the nanosized defects enclose quantized amount of magnetic flux.[12] A satisfactory model of such confinement mechanisms for interfaces inside HTS films is not yet available to date, due to two reasons: (i) the interaction concerns a huge number of confining elements (strongly interacting with each other and, in principle, exhibiting unknown relevant long range interactions); (ii) the distribution and size of the potential wells contains a certain degree of disorder and is unknown to a large extent.

The simplest way to describe such complex systems is to model the film as a random array of parallel uniform short Josephson junctions,[12] with statistically distributed junction lengths. Such a network can be thought as a one-dimensional array meandering in two-dimensional space. Moreover, the considered array must be regarded as the average high-J_c interface.[40,32]

In order to take into account the statistical distribution of the contact lengths, we consider a suitable probability density function $p(L)$. The critical current is obtained as the average, weighted by $p(L)$, of the critical current of the single junctions, each of them characterized by its own value of length L and magnetic thickness of the barrier Λ_0. The critical current of the single junction is described by the usual Fraunhofer-like expression.[41] The macroscopic critical current density is thus expressed by

$$J_c(B)=\int_0^\infty dL p(L) J_c(0)\left|\frac{\sin(\pi B\Lambda_0 L/\Phi_0)}{\pi B\Lambda_0 L/\Phi_0}\right|. \qquad (1)$$

The presence of vortices into the grains affects the value of Λ_0. The order of magnitude of Λ_0 for $B>B_{c_1}$ should match the distance between Abrikosov vortices in the junction electrodes: $\Lambda_0(B)=\zeta(\Phi_0/B)^{1/2}$.[12] Equation (1) can thus be rewritten as

$$J_c(B)=J_c(0)\int_0^\infty d\beta f(\beta)\left|\frac{\sin\beta B^{1/2}}{\beta B^{1/2}}\right|, \qquad (2)$$

where the variable $\beta=\pi L\zeta/\Phi_0^{1/2}$ summarize all the field-independent parameters and $f(\beta)=p[\beta\Phi_0^{1/2}/(\pi\zeta)]\Phi_0^{1/2}/(\pi\zeta)$. Here $J_c(0)$ is supposed to be the same for all the junctions. The AFM characterization shown in Fig. 3 suggests that the contact lengths have a well characterized mean value and both very low and very large L values are unlikely. This consideration leads to a bell-shaped probability density function and a simplicity criterion suggests $f(\beta)=k^2\beta e^{-k\beta}$. The length probability density distribution is then

$$p(L)=\frac{\pi^2\zeta^2}{\Phi_0}k^2 L\exp\left[-k\frac{\pi\zeta}{\Phi_0^{1/2}}L\right].$$

The main achievement of this treatment is that, in this case, Eq. (2) leads to an analytical result for the dependence of J_c on B:

$$J_c(B)=J_c(0)\frac{k^2}{k^2+B}\coth\left(\frac{\pi k}{2B^{1/2}}\right). \qquad (3)$$

In Fig. 8 we report the experimental data for sample (a) fitted by Eq. (3), with $J_c(0)$ and k as fitting parameters. The fitting procedure is remarkably successful in the low-temperature/high-current regime. Deviations from the model arise if the reduced temperature is increased over 0.53. The values of the fitting parameters for the three samples and different reduced temperatures are reported in Table I. As expected, the irradiation increases the value of the parameter k, leading to a probability density function $p(L)$ shifted towards lower L values, if one assumes that ζ is not significantly affected by irradiation. This means that extrinsic columnar defects break the pre-existing Josephson junctions of the intergranular network, leading to a network characterized by shorter Josephson-junction lengths.

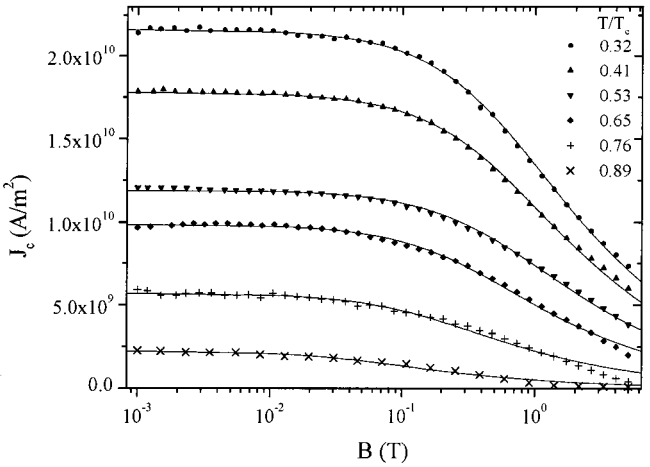

FIG. 8. Critical current density dependence on the magnetic field, at different reduced temperatures, for the sample (a). Solid lines represent the fitting of the experimental data by means of Eq. (3). The fitting parameters are reported in Table I.

In the model system $J_c(0)$ and k are independent fit parameters. In the real system it can be assumed that some correlation exists, because the irradiation induced defects are likely to create or modify the characteristics of the tunnel barrier. However, the dose dependence of $J_c(0)$ could be attributed to some damage phenomena at low fields. In this context, it seems that at higher dose the possible low field damage is shadowed by the positive influence of the defects.

D. Irreversibility line

Finally we turn to the irreversibility line (IL), i.e., to a regime of vanishing depinning critical currents. The inset of Fig. 9 shows that the effect of irradiation is a clear shift of the IL towards higher reduced temperatures and fields. This enhancement is remarkable if one considers that the preirradiation IL of these films is already steep. A general trend shown by the two irradiated samples at low fields is a curve steeper than that of the virgin sample. When the field is increased, sample (c) shows the evidence of a clear kink in the IL.

In order to interpret these data, it must be considered that at temperatures close to T_c the divergence of the coherence length increases the grain coupling and implies a weakening of the junction nature of the island boundaries.[42,31] In fact we analyze the IL in the framework of the phase transitions of the vortex lattice in a continuum medium already used in single crystals.[9] In the case of clean materials a melting transition $[t_m(B)=T_m(B)/T_c]$ shows up while in the case of correlated disorder a Bose-glass transition $[t_{\rm BG}(B)=T_{\rm BG}(B)/T_c]$ should be found. Starting from $t_m(B)$ one can determine the Bose-glass transition $t_{\rm BG}(B)$ for samples with columnar defects, by means of the relation

$$t_{\rm BG}(B)=\frac{t_m(B)+t_{on}\gamma}{1+\gamma}, \qquad (4)$$

where $\gamma=b_0^2[16d\xi_{ab}(0)({\rm Gi})^{1/2}]^{-1}$, d is the average distance between tracks, Gi is the Ginzburg number,[8] and b_0 is the

TABLE I. Values of the parameters obtained by fitting with Eq. (3) the critical current density dependence on the magnetic field. $J_c(0)$ is expressed in A/m^2 and k in $T^{1/2}$. Examples of fitting curves are reported in Fig. 8.

T/T_c	Sample (a) $B_\phi=0$	Sample (b) $B_\phi=0.3$ T	Sample (c) $B_\phi=1.5$ T
0.32	$J_c(0)=(2.162\pm0.002)10^{10}$	$J_c(0)=(1.465\pm0.001)10^{10}$	$J_c(0)=(2.38\pm0.04)10^{10}$
	$k=1.21\pm0.01$	$k=1.76\pm0.01$	$k=1.81\pm0.07$
0.41	$J_c(0)=(1.778\pm0.002)10^{10}$	$J_c(0)=(1.330\pm0.002)10^{10}$	$J_c(0)=(1.99\pm0.04)10^{10}$
	$k=1.18\pm0.01$	$k=1.60\pm0.01$	$k=1.57\pm0.09$
0.53	$J_c(0)=(1.191\pm0.002)10^{10}$	$J_c(0)=(1.203\pm0.003)10^{10}$	$J_c(0)=(1.45\pm0.05)10^{10}$
	$k=1.20\pm0.01$	$k=1.23\pm0.01$	$k=1.23\pm0.13$
0.65	$J_c(0)=(9.86\pm0.03)10^{9}$	$J_c(0)=(9.62\pm0.06)10^{9}$	$J_c(0)=(1.04\pm0.05)10^{10}$
	$k=0.91\pm0.01$	$k=0.93\pm0.02$	$k=1.08\pm0.06$

confining diameter. Equation (4) corresponds to Eq. (3) of Ref. 9, suitably modified by the introduction of the parameter t_{on}.[36] This parameter takes into account that the enhanced phase transition could present an onset point in the (T,B) plane not exactly coincident with T_c. Figure 9 shows the data for the film (c) (irradiated at $B_\phi=1.5$ T) fitted by Eq. (4), with γ and t_{on} as fitting parameters. The $t_m(B)$ curve was obtained as a polynomial fit from unirradiated-film data. We found $t_{on}=0.995\pm0.001$ and $\gamma=0.69\pm0.04$. The Bose-glass transition is extended up to $B=0.75\,\mathrm{T}\approx B_\phi/2$, where the characteristic kink appears, while at higher fields the IL slope decreases, in perfect agreement with findings of Ref. 9, concerning YBCO crystals crossed by columnar defects. The fitting parameter γ can be used to evaluate the dimensions of the confinement region b_0. By taking $\xi_{ab}(0)=1.2$ nm and $\mathrm{Gi}=0.004$,[9] we obtain $b_0=5.5$ nm, in remarkable agreement with the diameter expected for the irradiation-induced columns. We can hence conclude that for sample (c) a Bose-glass-like transition sets up at temperatures very close to T_c. These findings validate the hypothesis we made when we assumed the IL of the unirradiated sample as a good estimate of $t_m(B)$. As discussed above, this assumption implies that in the regime of vanishing J_c (high temperatures), the pinning provided by the extrinsic defects across the full surface of the film prevails over the pinning of as-grown correlated defects. In the case of sample (b), irradiated at the lower dose, the $B<B_\phi$ available data do not allow to extract the parameters mentioned before, although the IL shift towards higher temperatures and fields is out of the experimental errors.

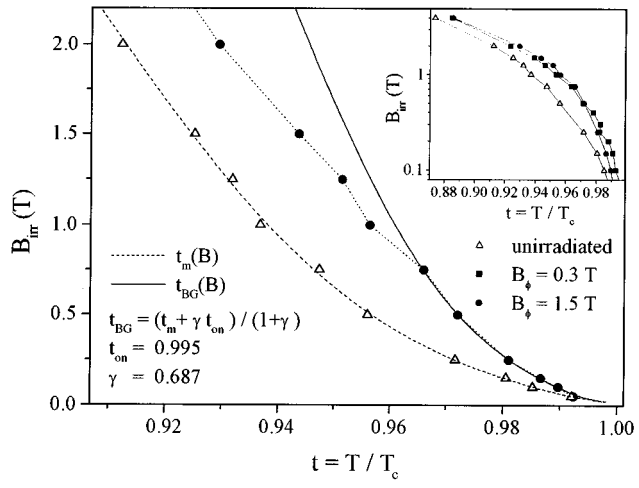

FIG. 9. Irreversibility line for the reference sample and the irradiated samples (inset). In the main figure, the fit of the $B_\phi=1.5$ T data by Eq. (4) is shown. Fitting parameters are also reported.

VI. CONCLUSIONS

We prepared partially deoxygenated YBCO films by appropriately varying the standard cooling process. The analysis of transport and structural properties converged to the conclusion that these samples present an island structure with defected grain boundaries. In fact, the presence of the ''tail regime'' in the zero-field $R(T)$ curve can be connected to the oxygen-deficiency revealed by Raman spectroscopy and to the island morphology revealed by AFM micrography.

In spite of a slight decrease of the critical temperature with respect to optimally doped samples, these oxygen-deficient samples exhibit large plateaulike features in the log-log $J_c(B)$ plots. In order to investigate what the defect network supporting high critical current paths is, we irradiated two samples with different doses of high-energy heavy ions. The lower dose corresponds to a columnar defect density close to the island density. The higher dose corresponds to column density five times higher than in the previous case.

We measured the critical current dependence on temperature and field for the three samples. All the data support the idea that the pinning properties of these films are dominated by the effects of correlated disorder, either intrinsic or extrinsic.

We analyzed two regimes: the high-current/low-temperature regime and the low-current/high-temperature regime. In the high current regime, the J_c vs B curves suggest the existence of an intergranular network where the grain boundaries contain high critical current density channels. In particular, a simple model, based on an array of Josephson junctions with statistically distributed lengths and field-dependent barrier thickness, optimally fits the experimental data. The intergrain network under such conditions must be the very same network carrying the highest J_c, and it does not have the characteristics of a weak link network.

Conversely, for temperatures close to T_c, the irreversibility line shift due to irradiation can be explained in terms of the Bose-glass model. Close to T_c, due to the diverging coherence length, the structure behaves almost as a continuum, in which the irradiation-induced columns, distrib-

uted along the full film surface, emerge as the effective pins.

The control of the superconducting properties of these films through either intrinsic defects or extrinsic defects costs in terms of T_c decreasing, also due to the large amount of irradiation-induced amorphous material. A solution to this problem could be the formation of ''surface'' correlated defects which do not cross the whole sample but extend themselves to a limited part of the thickness.[36] Investigations in this sense are in progress.

ACKNOWLEDGMENTS

The authors wish to thank A. Amato and the staff of the LNS-INFN for their help in the irradiation runs, and L. Tapfer (CNRSM-PASTIS) and P. Valisa (Instruments SA-Italia) for structural analysis. This work was partially supported by INFM under the project PRA ''High Temperature Superconductor Devices'' and by INFN under the project SURADDA.

[1] G. Doornbos, B. Dam, J. C. Martinez, R. Surdeanu, U. Poppe, and R. Griessen, Physica C **282–287**, 2303 (1997).
[2] J. C. Martinez, B. Dam, B. Stauble-Pumpin, G. Doornbos, R. Surdeanu, U. Poppe, and R. Griessen, J. Low Temp. Phys. **105**, 1017 (1996).
[3] T. Haage, J. Zegenhagen, J. Q. Li, H.-U. Habermeier, M. Cardona, Ch. Jooss, R. Warthmann, A. Forkl, and H. Kronmuller, Phys. Rev. B **56**, 8404 (1997).
[4] L. Civale, A. D. Marwick, T. K. Worthington, M. A. Kirk, J. R. Thompson, L. Krusin-Elbaum, Y. R. Sun, J. R. Clem, and F. Holtzberg, Phys. Rev. Lett. **67**, 648 (1991).
[5] V. Hardy, D. Groult, M. Hervieu, J. Provost, B. Raveau, and S. Bouffard, Nucl. Instrum. Methods Phys. Res. B **54**, 472 (1991).
[6] M. Konczykowski, F. Rullier-Albenque, E. R. Yacoby, A. Shaulov, Y. Yeshurun, and P. Lejay, Phys. Rev. B **44**, 7167 (1991).
[7] G. Blatter, M. V. Feigel'man, V. B. Geshkenbein, A. I. Larkin, and V. M. Vinokur, Rev. Mod. Phys. **66**, 1125 (1994).
[8] D. R. Nelson and V. M. Vinokur, Phys. Rev. B **48**, 13 060 (1993).
[9] L. Krusin-Elbaum, L. Civale, G. Blatter, A. D. Marwick, F. Holtzberg, and C. Feild, Phys. Rev. Lett. **72**, 1914 (1994).
[10] H. Hilgenkamp and J. Mannhart, Appl. Phys. Lett. **73**, 265 (1998).
[11] M. Prester, Supercond. Sci. Technol. **11**, 333 (1998).
[12] X. Y. Cai, A. Gurevich, I-Fei Tsu, D. L. Kaiser, S. E. Babcock, and D. C. Larbalestier, Phys. Rev. B **57**, 10 951 (1998).
[13] R. Surdeanu, R. J. Wijngaarden, B. Dam, J. Rector, R. Griessen, C. Rossel, Z. F. Ren, and J. H. Wang, Phys. Rev. B **58**, 12 467 (1998).
[14] I. Maggio-Aprile, C. Renner, A. Erb, E. Walker, and O. Fischer, Nature (London) **390**, 487 (1997).
[15] D. Zech, K. Conder, H. Keller, E. Kaldis, and K. A. Müller, Physica B **219–220**, 136 (1996).
[16] The dose equivalent field is the magnetic field which would be ideally required to fill each track with a flux quantum, i.e., $B_\Phi = n\Phi_0$, where Φ_0 is the flux quantum and n is the track density.
[17] J. F. Ziegler, J. P. Biersack, and U. Littmark, *The Stopping and Range of Ions in Solids* (Pergamon, New York, 1985), Vol. 1.
[18] V. Hardy, J. Provost, D. Groult, Ch. Simon, M. Hervieu, and B. Raveau, J. Alloys Compd. **195**, 395 (1993).
[19] Y. Zhu, R. C. Budhani, Z. X. Cai, D. O. Welch, M. Suenaga, R. Yoshizaki, and H. Ikeda, Philos. Mag. Lett. **67**, 125 (1993).
[20] M. Toulemonde, S. Bouffard, and F. Studer, Nucl. Instrum. Methods Phys. Res. B **91**, 108 (1994).
[21] P. V. Huong, Physica C **180**, 128 (1991).
[22] B. Li, C. Shelley, L. F. Cohen, A. D. Caplin, R. A. Stradling, W. Kula, R. Sobolewski, and J. L. MacManus-Driscoll, J. Appl. Phys. **80**, 2929 (1996).
[23] M. N. Iliev, P. X. Zhang, H. U. Habermeier, and M. Cardona, J. Alloys Compd. **251**, 99 (1997).
[24] E. Faulques, P. Mahot, M. Spiesser, T. P. Nguyen, G. Garz, C. Gonzales, and P. Molini, Phys. Rev. B **50**, 1209 (1994).
[25] G. Garz, E. Faulques, G. Le Roux, J. Schneck, and C. Gonzales, in *Applied Superconductivity*, edited by H. C. Freyhardt (DGM informationgesellschaft-Verlag, Oberursel, Germany, 1993), p. 541.
[26] A. Gurevich and L. D. Cooley, Phys. Rev. B **50**, 13 563 (1994).
[27] Y. Gao, K. L. Merkle, G. Bai, H. L. M. Chang, and D. J. Lam, Physica C **174**, 1 (1991).
[28] R. M. Schalk, K. Kundzins, H. W. Weber, E. Stangl, S. Proyer, and D. Bauerle, Physica C **257**, 341 (1996).
[29] Y. Zhu, Z. X. Cai, R. C. Boudani, M. Suenaga, and D. O. Welch, Phys. Rev. B **48**, 6436 (1993).
[30] J. R. Clem and A. Sanchez, Phys. Rev. B **50**, 9355 (1994).
[31] J. Jung, H. Darhmaoul, and H. Yan, Supercond. Sci. Technol. **11**, 973 (1998).
[32] R. Fehrenbacher, V. G. Geshkenbein, and G. Blatter, Phys. Rev. B **45**, 5450 (1992).
[33] E. Mezzetti, E. Crescio, R. Gerbaldo, G. Ghigo, L. Gozzelino, and B. Minetti, J. Supercond. (to be published).
[34] U. C. Tauber and D. R. Nelson, Phys. Rev. B **52**, 16 106 (1995).
[35] L. Krusin-Elbaum, L. Civale, J. R. Thompson, and C. Feild, Phys. Rev. B **53**, 11 744 (1996).
[36] E. Mezzetti, R. Gerbaldo, G. Ghigo, L. Gozzelino, and L. Gherardi, Phys. Rev. B **59**, 3890 (1999).
[37] T. Bauch, S. Weiss, H. Haensel, A. Marx, D. Koelle, and R. Gross, IEEE Trans. Appl. Supercond. **7**, 3605 (1997).
[38] M. A. Itzler and M. Tinkham, Phys. Rev. B **51**, 435 (1995).
[39] E. Mezzetti, S. Colombo, R. Gerbaldo, G. Ghigo, L. Gozzelino, B. Minetti, and R. Cherubini, Phys. Rev. B **54**, 3633 (1996).
[40] J. Rhyner and G. Blatter, Phys. Rev. B **40**, 829 (1989).
[41] A. Barone and G. Paternò, *Physics and Applications of the Josephson Effect* (Wiley, New York, 1982).
[42] J. R. Clem, B. Bumble, S. I. Raider, W. J. Gallagher, and Y. C. Shih, Phys. Rev. B **35**, 6637 (1987).